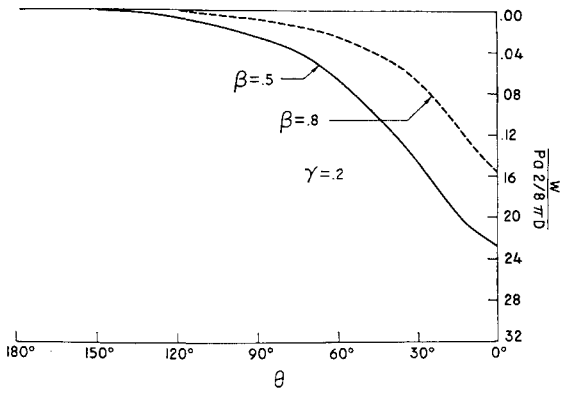

Fig. 3 Deflection along the circle of βa radius.

$$A_n + B_n + C_n + D_n = 0 \quad (12a)$$

$$A_n n(n-1)(1-\nu) + B_n n(n+1)(1-\nu) + C_n(n+1)[(n+2) - \nu(n-2)] + D_n \times (n-1)[(n-2) - \nu(n+2)] = 0 \quad (12b)$$

$$A_n(\gamma^2)^n + B_n + C_n(\gamma^2)^{n+1} + D_n\gamma^2 + (\gamma^2)^n \left[\frac{1}{\beta^n}\langle(\beta^2)^n - 1\rangle \times \frac{(\gamma^2+\beta^2)}{n} - \frac{1}{\beta^{n+1}}\langle(\beta^2)^{n+1} - 1\rangle \frac{\beta\gamma^2}{n+1} - \frac{1}{\beta^{n-1}}\langle(\beta^2)^{n-1} - 1\rangle \frac{\beta}{n-1} + \frac{2(1-\beta^2)\beta^n}{2n+1+\nu} \times (1-\nu^2)\right] = 0 \quad (12c)$$

$$A_n(\gamma^2)^{n-1}n(n-1)(1-\nu) + B_n\gamma^{-2}n(n+1)(1-\nu) + C_n(\gamma^2)^n(n+1)[(n+2) - \nu(n-2)] + D_n(n-1)[(n-2) - \nu(n+2)] + (\gamma^2)^n\left[(n+1)\langle(n+2) - \nu(n-2)\rangle\left(\frac{1}{\beta^n}\langle(\beta^2)^n - 1\rangle\frac{1}{n} - \frac{1}{\beta^{n+1}}\langle(\beta^2)^{n+1} - 1\rangle\frac{\beta}{n+1} - \frac{2(1-\beta^2)\beta^3}{2n+1+\nu}\right) + n\langle(n-1)(1-\nu)\rangle\left(\frac{1}{\beta^n}\langle(\beta^2)^n - 1\rangle \times \frac{\beta^2}{n} - \frac{1}{\beta^{n-1}}\langle(\beta^2)^{n-1} - 1\rangle \frac{\beta}{n-1} + \frac{2(1-\beta^2)\beta^3}{2n+1+\nu}\right)\right] = 0 \quad (12d)$$

Results

In Figs. 2 and 3 the deflection along a radial line $w = w(\rho)$ and along a circumferential line $w = w(\theta)$, respectively, have been plotted for $\gamma = 0.2$ and for $\beta = 0.5, 0.8$. It is seen that the deflection of the region diametrically opposite to the point of application of load is, for all practical purposes, nil, and that the width of this area is a sector of about 90°. It can thus be inferred that in this region the stress resultants and stresses are very small.

A comparison of the result obtained here with those of Ref. 1 for the clamped plate indicates that the deflection and the deflection zone are twice as large as for the clamped case.

References

[1] Amon, R. and Widera, O. E., "Clamped Annular Plate under a Concentrated Source," *AIAA Journal*, Vol. 7, No. 1, Jan. 1969, pp. 151–153.

[2] Timoshenko, S. and Woinowsky-Krieger, S., *Theory of Plates and Shells*, McGraw-Hill, New York, 1959.

[3] Reissner, E., "Über die Biegung der Kreisplatte mit exzentrischer Einzellast," *Mathematische Annalen*, Vol. 3, 1935, pp. 777–780.

[4] Washizu, K., "On the Bending of Isotropic Plates," *Transactions of the Japan Society of Mechanical Engineers*, Vol. 18, 1952, pp. 41–47.

[5] Dundurs, J. and Lee, T. M., "Flexure by a Concentrated Force of the Infinite Plate on a Circular Support," *Journal of Applied Mechanics*, Vol. 30, 1963, pp. 225–231.

A Planview Shadowgraph Technique for Boundary-Layer Visualization

ENRIQUE J. KLEIN*
NASA Ames Research Center, Moffett Field, Calif.

As part of a study on the formation and growth of disturbances generated by spark discharges into a laminar boundary layer,[1] an optical arrangement was devised to observe such disturbances viewed against the surface of the model rather than across its edge as in conventional systems. This was achieved by using a double-pass focused shadowgraph system, incorporating in the wind-tunnel test section a plane mirror that served simultaneously as a flat-plate model. Tests were made in the Ames 1- by 3-ft supersonic wind tunnel.

The optical arrangement is shown schematically in the diagram of Fig. 1. It consisted of a spark gap with interchangeable apertures, a beam splitter, a first surface spherical mirror of 18-in. diam and 120-in. focal length, a flat mirror model, as well as a focusing lens of 52.5-in. focal length, a shutter and aperture, a camera box of adjustable length, and a 4- by 5-in. film holder, all mounted on an optical bench. In practice, the beam splitter was replaced by a first surface mirror to increase the lighting efficiency. It was set at an angle of 45° and slightly off axis to avoid intercepting the light rays returning from the test section. The optical paths from the spark gap aperture and the focusing lens to the spherical mirror were both set at 120 in., the focal distance of the mirror. The focal length of the focusing lens and the length of the camera box were calculated to obtain an image reduction of 3:1 with the model surface in focus. The model was a flat plate with a 6- by 10-in. surface and a sharp leading edge. It was made of stress-relieved mild steel, coated with nickel to obtain an appropriate hardness, and polished to $\lambda_D/4$ flatness. This surface later was coated with a layer of vacuum-deposited aluminum and a protective layer of silicon monoxide. A grid of 0.5-in. spacing was painted on this surface for reference.

In this optical system, the light from the spark gap first reaches the spherical mirror, where it is reflected as a parallel beam of light to the test section. At the mirror model, it is reflected back to the spherical mirror and from there through the focusing lens, shutter, and aperture to the film. To obtain a shadowgraph of the density variations in the boundary layer on the mirror model, it becomes necessary to focus the system not on the surface of the mirror model but on a plane closer to the spherical mirror. Ideally, focusing on the inside surface of the wind-tunnel window would eliminate the image of the density gradients of the window boundary layer while permitting a clear view of the density gradients of the model boundary layer.

Received December 15, 1969. This investigation was accomplished during the author's tenure of a National Research Council Postdoctoral Research Associateship supported by NASA. The author is indebted to G. B. Schubauer of the National Bureau of Standards, as the concept for this technique originated in a discussion with him. I also would like to express my appreciation to R. M. Brown, who carried out the analysis for the optical system.

* National Research Council—Research Associate. Associate Fellow AIAA.

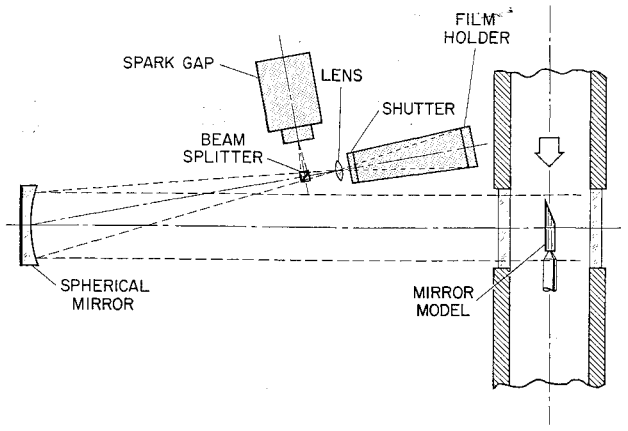

Fig. 1 Planview shadowgraph optical arrangement.

The "in focus" distances between the lens and the film plane were obtained by focusing on an incandescent miniature light bulb located first at the inside surface of the wind-tunnel window and then at the model surface. These distances were 103 cm for the window surface and 101 cm for the model surface. An additional optimization test was made to determine the distance between the lens and the film plane at which the shadowgraph image would be strongest for the model surface relative to the image for the window surface. This was done by taking shadowgraphs of two lit candles, each next to one of the two surfaces and laterally offset to permit the identification of the density patterns from their flames. Results showed that while discrimination was never very marked, the optimum setting was indeed obtained when the window surface was in focus. When the focused plane lay even closer to the spherical mirror, both shadowgraph images were found to become more intense simultaneously.

The shadowgraph of Fig. 2 shows the mirror model in the wind-tunnel test section with no airflow and the signature from a hemispherical shock wave surrounding the electrode holder (black button). This shock wave was generated by a single spark from a pair of electrodes embedded in a boron nitride holder flush with the model surface. The shadowgraph was taken 50 μsec after the spark discharge, the energy input to the spark was 1.45 joules, and the test was carried out at a pressure of 255 torr. The leading edge, on the left side, and the area surrounding the electrode holder appear distorted due to some lack of surface flatness.

With the wind tunnel operating at $M_\infty = 3.53$, the shadowgraph in Fig. 3 shows the disturbance generated by a spark of 1.45 joules energy at a time interval of 50 μsec and a static pressure of 35 torr. Now, the signature of the spherical shock

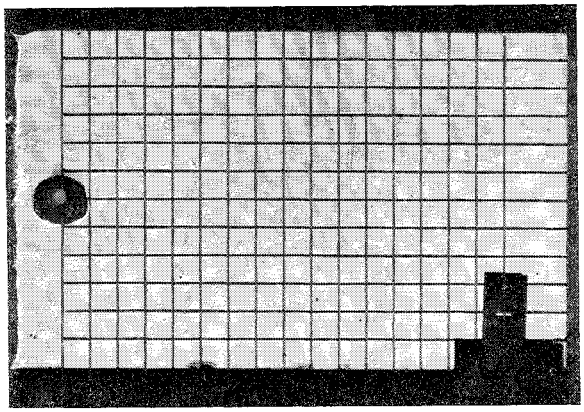

Fig. 2 Shadowgraph of a hemispherical shock wave generated by a spark discharge at the surface of the mirror model with no airflow, 255-torr pressure, energy input of 1.45 joules, time delay of 50 μsec.

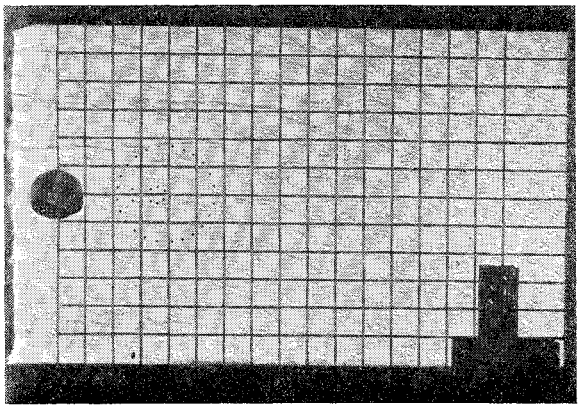

Fig. 3 Shadowgraph of the disturbances generated by a spark discharge at the surface of the mirror model at $M_\infty = 3.35$, $p_s = 35$ torr. Energy input, 1.45 joules; time delay, 50 μsec. The black dots indicate the position of the disturbances.

wave is displaced 4.6 cm downstream of the electrode location, and a disturbance can be discerned in the center of the circle and trailing upstream of it. Both disturbances are shown outlined by black dots. A turbulent structure is also visible over the entire surface. Since the testing conditions were known to result in a partly laminar and partly turbulent boundary layer over the surface of the model, this over-all turbulence must correspond to the window boundary layer. The near horizontal trails on the upper left side are the image of oil streamers on the inside surface of the wind-tunnel window. It was found that, during wind-tunnel operation, the slight variation in the angle of the model surface due to the deformation of the model supporting sting had to be compensated by adjusting the optical bench to render the model visible again on the film area. No difficulties were experienced with vibration since the discharge of the spark gap, which is of the order of 0.1 μsec, was fast enough to stop any low-frequency motion.

To allow a comparison of the planview disturbance patterns with conventional profile shadowgraphs, Fig. 4 shows results from similar experiments carried out in the same wind tunnel, using a half-cylinder model with a sharp leading edge[1] and a single-pass focused shadowgraph arrangement. In Fig. 4, a) is a static test at ap ressure of 116 torr, and b) is a test at $M_\infty =$

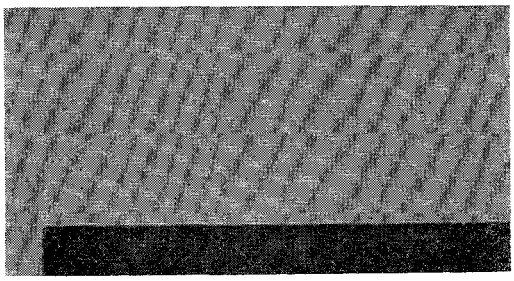

a) Static test, $p_s = 116$ torr.

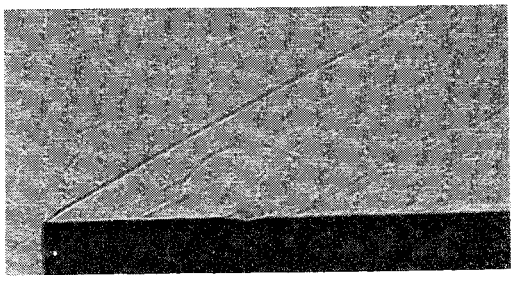

b) $M_\infty = 2.36$, $p_s = 115$ torr.

Fig. 4 Shadowgraph of the disturbances generated by a spark discharge at the surface of a half cylinder model. Energy input, 1.45 joules; time delay, 50 μsec.

2.36 at a static pressure of 115 torr. In both tests, the energy input to the spark was 1.45 joules, and the time delay 50 μsec. For the tunnel in operation, similarities between the disturbances viewed in planview and in profile are clearly apparent.

The main drawback of the planview shadowgraph technique in its present form proved to be its inability to show anything but the strongest boundary-layer disturbances, due to the masking effect of the boundary layer on the inside surface of the wind-tunnel window. It would be highly desirable to perfect this technique to the point where the finer details of the boundary layer could be observed in planview. For example, boundary-layer transition could be observed similarly to the way in which Emmons observed the appearance of turbulent spots in shallow water.[2] To achieve this, it is suggested that a) the focal length of the spherical mirror and consequently its f-stop be increased substantially to reduce the depth of field and permit minimizing the disturbance from the window boundary layer, and b) that the turbulent boundary at the near wind-tunnel wall be bled away upstream of the window, leaving only a thin, newly formed, boundary layer covering the inside surface of the window. While neither of these refinements is simple or inexpensive, the potential rewards in terms of basic information on boundary-layer behavior may still warrant their implementation, particularly since no other techniques with such capabilities are known.

References

[1] Klein, E. J., "Excitation of Boundary-Layer Turbulence Through Spark Discharges," NASA Ames Research Center (report in preparation).

[2] Emmons, H. W., "The Laminar-Turbulent Transition in a Boundary Layer-Part I," *Journal of the Aeronautical Sciences*, Vol. 18, No. 7, July 1951, pp. 490–498.

Condensation in Carbon Dioxide Jet Plumes

ALFRED E. BEYLICH*
NASA Marshall Space Flight Center, Huntsville, Ala.

CONSIDERABLE difficulties exist in calculating the flowfield of jet plumes such as those that issue from the attitude control engines of space stations, especially if condensation and changes in the specific heats occur in the flow. In order to obtain information about the condensation in these plumes, a simple experimental approach was made.

A model nozzle (0.56 mm throat diam, 11° half angle, and 40:1 exit to throat area) was used to produce a CO_2 jet plume in a vacuum chamber with LN_2 cooled cryogenic panels. With a chamber background pressure of about 10^{-4} torr, a ratio of stagnation to background pressure, p_0/p_∞, could be maintained up to 10^8. Nozzle wall temperature T_w and stagnation temperature T_0 were controlled. The use of CO_2 has, apart from the ease of cryopumping very large mass flows, importance because 40–60% of actual combustion products in control engines consist of CO_2 plus H_2O. Thus condensation effects in the flow can be fairly well simulated and studied.

Received October 27, 1969; revision received February 4, 1970. Research was accomplished while the author held a NRC Postdoctoral Resident Research Associateship supported by MSFC. The author wants to thank J. L. Sims from MSFC for making available his calculations and the staff of the Aero-Astrodynamics Laboratory for making these experiments possible.

* Resident Research Associate; presently on leave from Technische Hochschule, Aachen, Germany.

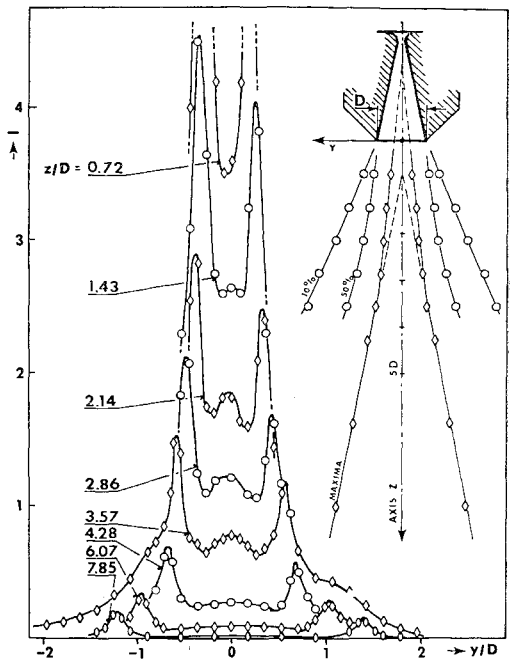

Fig. 1 Distribution of scattered light intensity (arbitrary units) at different distances z from the nozzle exit for stagnation pressure P_0 = 8 bar, stagnation temperature T_0 = 293°K, and chamber background pressure $P_\infty = 10^{-4}$ torr.

Light scattering, which is a simple and often applied method,[1,2] was used to detect the condensation. A He-Ne-laser and a photomultiplier were arranged with each of their optical axes perpendicular to the plume axis. The nozzle could be moved in three directions so that it was possible to measure the intensity of the scattered light at different points in the flow. By rotating the plane of polarization of the incident beam, one is able to make a first estimation about the particle size. In all experiments, this yielded a typical Rayleigh-type scattering. Thus the particle radius must be smaller than 6328 Å/2π. In the case of Rayleigh scattering one can only measure the product $n \cdot r^6$, where n is the number density and r a weighted mean radius of the condensed clusters. Thus knowledge of the amount of condensed mass is necessary to interpret the intensity measurements. In some cases this information can be obtained from calculation. Absolute values of $n \cdot r^6$ were obtained by comparing the intensity of the scattered light with the intensity of one pinhole of known size.

For an isentropic expansion[3] the vapor pressure line is crossed at about Mach 2, for p_0 = 1 — 10 bar and T_0 = 300°K, thus condensation should start slightly downstream the throat. The supersaturation required for starting the nucleation will move the condensation zone a small distance more downstream, but it will remain inside the nozzle. Thus condensation should, at low temperatures T_0, always be detected right up to the nozzle exit.

A survey of the intensity measurements in the jet plume is given in Fig. 1. A remarkable property of the scans arcoss the plume are the two peaks that appear on either side of the axis. The position of these maxima relative to the nozzle is shown on the right-hand side of Fig. 1, as well as the lines of 50 and 10% intensity, compared to the intensity $I(z,y = 0)$ on the axis. The influence of the stagnation temperature, T_0, on the intensity distribution across the plume at a fixed distance of 2.86 nozzle exit diam D is given in Fig. 2. With rising temperature T_0 the peaks move closer together; finally they merge to one peak and two additional side peaks appear. If one keeps the stagnation temperature constant